

Chemical and biological sensors

FluoCount: An Efficient and Accurate Cells and Bioparticles Enumeration Mobile Application for Portable Fluorescence Microscopes

Muhammad Nabeel Tahir^{1,*} , Yongyu Xie¹ , Muhammad Ahsan Sami¹ , Rasika Punde¹ , and Umer Hassan^{1,2,**} 

¹Department of Electrical and Computer Engineering, Rutgers, The State University of New Jersey, Piscataway, NJ 08854 USA

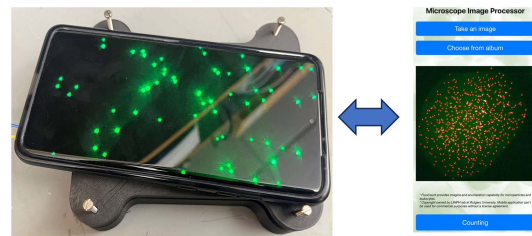
²Global Health Institute, Rutgers, The State University of New Jersey, Piscataway, NJ 08854 USA

*Graduate Student Member, IEEE

**Member, IEEE

Manuscript received 7 February 2024; accepted 25 February 2024. Date of publication 28 February 2024; date of current version 12 March 2024.

Abstract—Fluorescence microscopes are widely used to detect fluorescent objects in a biological sample. However, traditional benchtop fluorescence microscopes are limited to high cost and nonportability. Recently, smartphone-based fluorescence microscopes (SFMs) have been developed, which capture images using a smartphone camera with the help of an external optical device and serve as an inexpensive and portable alternative. However, to analyze the images and get the accurate count of bioparticles, external software and computational resources are required; moreover, the lack of single and clustered count capabilities in SFMs without relying on an image library limits the use of SFMs. Here, we present an automated method as a mobile application with the ability to provide the bioparticle counts at the point of care by imaging human leukocytes and fluorescent microparticles. The application employs efficient image processing techniques that result in faster automated counting and reduced computational cost while providing comparable counts to industrial and academic standards. Compared with counting results calculated by ImageJ, a correlation coefficient of $R^2 > 0.99$ was observed along with the average relative error of $\sim 0.5\%$ on different kinds of fluorescent images.



Index Terms—Chemical and biological sensors, bioparticles, image processing, leukocytes, smartphone fluorescent microscopy (SFM).

I. INTRODUCTION

Fluorescence microscopy has emerged as a critical tool in the field of biomedical and clinical diagnosis as it enables the visualization of molecules in the cells or different types of cells with high sensitivity and specificity [1]. It combines the fluorescent capabilities of a compound microscope and the magnifying capabilities of a light microscope providing a reliable resource for monitoring and imaging a biological sample. The applications of fluorescence microscopes are not only limited to clinical settings but span a wider area of science, e.g., environmental monitoring, agriculture, botany, and material science [2], [3]. By adding multiple fluorophores in a biosample, fluorescence microscopy can help in identifying different target species at the same time [4]. Apart from fluorescence microscopes, cell flow cytometers and hematology analyzers are typically used in clinical laboratories to enumerate the total population of cells in a processed blood or biological sample. This equipment provides the accurate results but at the expense of high equipment and maintenance costs resulting in the use of highly sophisticated laboratories. The benchtop fluorescence

microscopes provide a relatively cheaper solution to the expensive bioparticle counting devices, although they require expensive image processing software in terms of cost and computation to generate equivalent results. Due to higher costs and the need for specific training and infrastructures the benchtop fluorescent microscopes, scientists have to rely on the manual counting of bioparticles, which consumes time and is prone to human processing errors [5].

Smartphone-based fluorescence microscopes (SFMs) have offered an efficient yet inexpensive alternative solution to benchtop microscopes and can be used not only in clinical laboratories but at the point of care as well [6]. The cutting-edge camera systems in modern smartphones enable the use of SFMs in the detection of various biomarkers, including nucleic acids and proteins [7], [8]. Moreover, SFMs have also been employed to detect parasites [9], fluorescently tagged bioparticles [10], and antibody-expressed human leukocytes [11], [12]. Although, with the advent of SFMs, access to smart imaging systems has been made available even in limited resource settings, the technology still suffers from the bottleneck of image analysis applications. The commercially available software is expensive and cannot be used with mobile devices. The mobile applications available for free do not process images rather are digital click counters. Herein, we present a mobile application powered by sophisticated image processing algorithms to count the number of cells/bioparticles in images captured by SFMs. The application harnesses the image processing capabilities of modern smartphones and provides the accurate count of cells with a low computational cost at the point of care.

Corresponding author: Umer Hassan (e-mail: umer.hassan@rutgers.edu).

Muhammad Nabeel Tahir, Yongyu Xie, and Muhammad Ahsan Sami contributed equally to this work.

Associate Editor: S.-R. Kothapalli.

Digital Object Identifier 10.1109/LSENS.2024.3371209

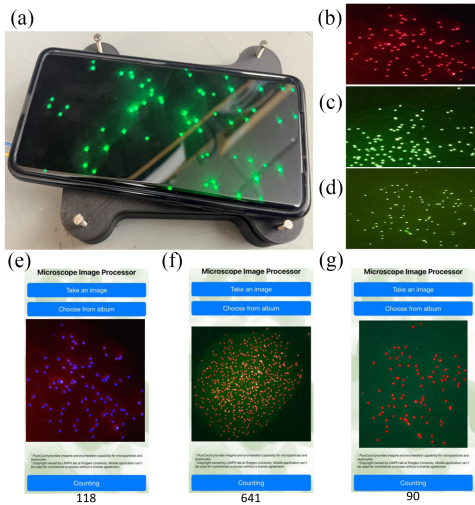


Fig. 1. (a) Experimental setup used in the study. (b) Red fluorescent beads sample image. (c) Green, fluorescent beads sample image. (d) White blood cell image. (e) Red beads counted using the application. (f) Green beads counted using the application. (g) White blood cells counted using the application.

II. METHODS AND MATERIALS

A. Experimental Setup and Sample Preparation

The experimental setup employs an SFM, as discussed in the study [1]. The SFM consists of two main components: the top portion and the bottom portion. The top portion houses a 3.1 mm optical filter (from Edmund optics stock # 87-165), a magnifier, and a slot for the smartphone. The bottom portion contains the cavities for the sample placement, the laser diode holder, and the power batteries. Fig. 1(a) shows the actual experimental setup used in this letter. A blue LED (Product # 516-2800-1-ND) was used to illuminate the sample surface. The entire SFM assembly was 3-D printed with four slots designed for the screws to adjust the SFM focus on the z-axis. Moreover, an optical filter with a center wavelength of 470 nm and a bandwidth of 40 nm was used to prevent the unwanted wavelengths from passing through the sample plane. To capture the images, a Samsung Galaxy S9+ Ultra phone was used. To optimally excite the sample surface, 3.3 V was used as the excitation voltage following the results published in the previous study [1].

To evaluate the performance of the experimental setup, the developed counting algorithm, and the mobile application, the experiments were performed using the synthetic polystyrene-based microspheres with different fluorophores and actual human leukocytes. The green, fluorescent microparticles were procured from Bangs Laboratories (Product # UMDG003) with an average diameter of 8.3 μm to mimic the size of the human leukocytes. The green, fluorescent beads at various concentrations were added to 1 \times PBS solution to create a diluted sample and 1 μL of the sample was imaged using the SFM setup. Varying the concentration of fluorescent beads helps in identifying the detection limits of both SFM and the counting algorithm. The collected images were used to create a green, fluorescent beads dataset containing 55 images. Similarly, the sample solutions of red fluorescent beads were prepared at different concentrations of beads in 1 \times PBS solution, and 1 μL of the sample was imaged. The red fluorescent beads were procured from Thermo Fisher (Product # F8834) with an average diameter of 10 μm . A dataset of red fluorescent bead images was prepared containing a total of seven images and later was used in evaluating the performance of the developed solution.

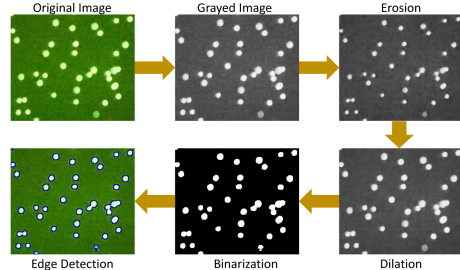


Fig. 2. Image processing pipeline flow diagram.

The preparation of the human leukocyte sample required further processing as it was prepared from the whole blood sample. The human blood samples of seven subjects were obtained from the Robert Wood Johnson Hospital in New Jersey following the approved guidelines of the Institutional Review Board (IRB) at Rutgers University (IRB application: Pro2018002356). To extract the leukocytes from the whole blood, one red blood cell lysis buffer was added to a 15 mL centrifuge tube along with 100 μL of whole blood. The solution was incubated at room temperature for 10 min and 2 mL of 1 \times PBS buffer was added to stop the lysing. The sample was centrifuged at 300 g for 5 min and the supernatant was removed leaving behind the pellet of the leukocytes. The extracted leukocytes were suspended in the RPMI 1640 medium and mixed gently to achieve a uniform concentration of the cells. A 3 μL of green nuclear stain SYTO 16 procured from ThermoFisher (Product # S7578) was added to the 1 mL 1 \times PBS buffer to prepare the cell-staining solution. A final sample was prepared by adding the cell-staining solution and leukocyte solution in a 1:1 and was incubated in the dark for 15 min. A 1 μL of the stained cell solution was imaged using the SFM setup resulting in a dataset of seven images. All three datasets were then used to assess the performance of the developed mobile application. Fig. 1(b)–(d) shows the images of green, red, and leukocytes imaged using the SFM setup. ImageJ [13], an open-source, state-of-the-art image processing software, was used to generate the control data. The image is converted to a grayscale; then, a threshold slider is used to manually select the pixels within a certain threshold that only contain the cells or particles. Then, analyzing the particle button generates the particle counts using an automated predefined algorithm.

B. Image Processing for Bioparticle Counting

To improve the efficiency of the counting process, an image processing pipeline was designed, as shown in Fig. 2. A colored image acquired from the smartphone was first converted to grayscale to reduce the complexity of the image processing and counting algorithms and overall computational cost. Since we are interested in the structural information in the image, i.e., the bioparticle shape, the grayscale image highlights the shape feature, hence facilitating the object or edge detection algorithms. In the second stage of the pipeline, a morphological operation called erosion is applied to the grayscale image. The erosion operation erodes the boundaries of the foreground pixels (i.e., white pixels) and reduces the size of the objects and noise. Since there is a possibility that the bioparticles form a group even after preparing a uniform concentration sample, the erosion operation helps in defining the clear boundaries of all the objects, thus isolating and identifying the particles in a group. Moreover, the erosion step minimizes the false positive rate, as the objects with a significantly smaller size than the target particles are either removed or reduced to negligible features. The erosion operation is followed by another

morphological operation called dilation. Dilation adds pixels to the boundary of an object, thus increasing the size of that object. In image processing pipelines, the dilation is used as a complementary operation to the erosion. Since erosion removes the small unwanted objects in the image, the dilation enlarges the boundaries of the remaining targeted objects, hence helping in improving the efficiencies of the edge detection algorithms. An image binarization step is applied after the dilation operation. The binarization step converts the image into a bilevel document, hence segmenting the foreground (white pixels) and background (black pixels). During this process, the pixels in the grayscale image that are below a certain threshold are set to zero, while the pixels that are higher than the threshold are set to 1 or 255. The threshold value is selected automatically using Otsu's method, as discussed in [13]. Finally, an edge detection algorithm is applied to the binary image to find the boundaries of the bioparticles in the image. A topological structure extraction algorithm has been employed, as presented in [14]. The algorithm detects the contours in an image. The contours are the boundary pixels that have the same intensity joined in a curve. Once the boundaries of each object in the image are detected, the algorithm returns the list of contours or boundaries containing the location (x, y) of each pixel in that boundary. Once the boundaries of the objects are known, the information can be used to count the number of objects or bioparticles in the image, the details of which are provided in Section II-C.

C. Counting Algorithm and Mobile Application

At the last stage of the image processing pipeline, a rough estimate of the total number of bioparticles can be made in the image by counting the distinct boundaries in the list returned by the edge detection algorithm. However, the estimate is not accurate when processing the larger concentration of the bioparticles, as the probability of objects bonding together to form groups or lumps increases, as discussed in the previous sections. Therefore, a sophisticated algorithm is required to segment the bioparticles into groups of multiple objects. Through experimental results obtained from the images, as shown in Fig. 1(b)–(g), it was observed that, if the total number of particles in the image is higher than roughly 100 particles, the groups or overlaps start to appear. A threshold of 100 was selected for the image to be considered eligible as an input of the counting algorithm. The counting algorithm designed in this study is shown in Algorithm 1. First, all the contours are sorted based on the size (area) of the objects. A threshold defining the minimum size of a cluster is calculated by first getting the area of an object whose size is at the 75th percentile and multiplying by 1.5 to estimate the final threshold for a possible group or lump object. The contours with an area larger than the selected threshold will be considered potential groups of multiple bioparticles, and the total number of particles is updated using the equation shown on line 10 in Algorithm 1. Once all the bioparticles are analyzed, a final estimate is calculated by taking the average of contours returned by the edge detection algorithm and bioparticle counting algorithm. Using the designed algorithm and image processing pipeline, a mobile application was developed with the ability to process the image captured at the time of the experiment or captured earlier. Fig. 1(e)–(g) shows the results of red, green, and leukocyte images processed using the developed mobile application.

III. RESULTS AND DISCUSSION

The datasets collected during the experimentation were used with ImageJ and a mobile application to generate the cell counts. The resulting information was used to perform the correlation and Bland–Altman analysis. The correlation plots were generated to show the

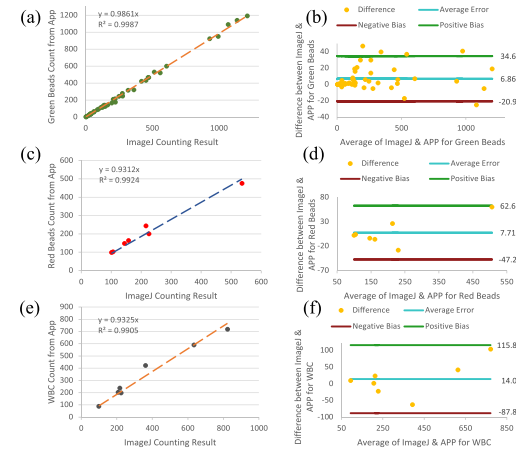


Fig. 3. (a) Correlation plot of green beads counted using application versus ImageJ. (b) Bland–Altman analysis plots of green beads data. (c) Correlation plot of red beads counted using application versus ImageJ. (d) Bland–Altman analysis plots of red beads data. (e) Correlation plot of white blood cells counted using application versus ImageJ. (f) Bland–Altman analysis plots of white blood cell data.

Algorithm 1: Counting Algorithm.

```

Input: all contours with area information saved in an array of
contours
Output: the counted number of bioparticles
1: org = contours.size ()
2: num = org
3: if org > 100 then
4:   contours.sort (based on size)
5:   index = 0.75 × num
6:   threshold = 1.5 × contours .get (index)
7:   for i = 0 to org do
8:     tmp = contours.get(i)
9:     if temp > threshold then
10:      num = num. + tmp/threshold — 1
11:    end if
12:   end for
13: end if
14: return (org + num)/2

```

correlation between the results of the three datasets processed using ImageJ and the developed application, as shown in Fig. 3(a), (c), and (e). It can be observed that the results generated by the application highly correlate to the results of ImageJ with correlation coefficients $R^2 > 0.99$ for all three datasets. The Bland–Altman are the scatter plots of the difference and average results of both ImageJ and the proposed application, as shown in Fig. 3(b), (d), and (f). The green beads and red beads datasets exhibit lower values of mean difference (bias) in Bland–Altman plots as compared with the doubled bias in the case of actual leukocyte data. Although the values of bias are not zero, since each image contains hundreds of bioparticles, the difference is negligible and can be ignored. The limits of agreement, although not narrow, still encompass 95% of the difference data with few exceptions of outliers in green beads data. The green beads dataset consisted of unwanted fluorescent artifacts in the image due to scattering of the light and processing errors, which resulted in higher counts with ImageJ, as fewer noise reduction filters were applied. The plots suggest that the developed application generates results that highly correlate with the ImageJ results, are within the agreeable difference range, and can be

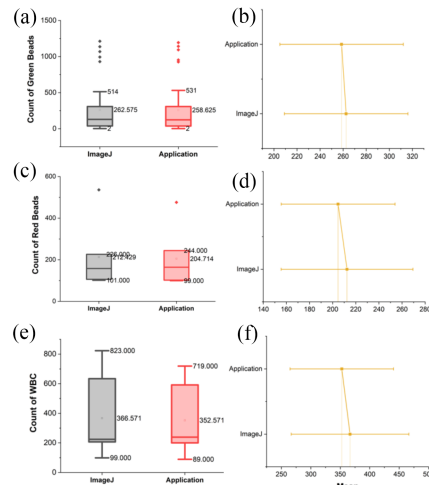


Fig. 4. (a) Box plot of green beads counted using application versus ImageJ. (b) Tukey plot analysis plots of green beads data. (c) Box plot of red beads counted using application versus ImageJ. (d) Tukey plot of red beads data. (e) Box plot of white blood cells counted using application versus ImageJ. (f) Tukey plot of white blood cell data.

considered as an effective alternative to academic standards, providing the results at the time of experimentation.

Moreover, the box plots were generated as shown in Fig. 4, and a statistical test ANOVA was performed to measure the statistical difference between the results of ImageJ and the designed application. The one-way ANOVA yielded the values of (p -value = 0.95 and F -value = 0.0027), (p -value = 0.92 and F -value = 0.0105), and (p -value = 0.91 and F -value = 0.011) for green beads, red beads, and leukocytes, respectively, highlighting that ImageJ and application generate results with no significant statistical difference. Tukey's plots were generated to show the difference if it exists between the mean results of ImageJ and the application. A significance level of $\alpha = 0.05$ was used for the tests. Tukey's tests suggest that the performance of the developed counting application is comparable to the ImageJ(control). Moreover, the developed mobile application only takes up to 5 s to generate the count in an image. The FlouCount algorithm generated comparable results to previous machine learning based particle counting studies done before [15]. Strengthening the claim that the application can serve as an effective alternative at the site of experimentation without requiring any further processing or data transfer hassle.

IV. CONCLUSION

A mobile application with low computational cost image processing techniques was developed and used on the SFM images to analyze the performance and capability of the application. The datasets were also analyzed using an open-source image processing software ImageJ. The correlation and Bland–Altman analyses were performed showcasing the high correlation $R^2 > 0.99$ and lower average mean differences. Further statistical analyses were performed using one-way ANOVA and Tukey's test, which depicted a higher p -value > 0.99 and a lower

average difference between the results of the ImageJ (control) and developed application. The results suggest that our solution can be effectively used as an alternative in clinical settings and at the point of care to detect and count fluorescent bioparticles. In the future, we aim to enhance the capability of the application by incorporating machine learning algorithms to count cells within the clusters and with nonuniform boundaries.

ACKNOWLEDGMENT

This work was supported in part by the National Science Foundation (Award # 2002511 and 2315376) and in part by New Jersey Health Foundation Grant. The authors would like to thank the Department of Electrical and Computer Engineering and Global Health Institute at Rutgers, The State University of New Jersey, for their support.

This work involved human subjects in its research. Approval of all ethical and experimental procedures and protocols was granted by Rutgers Institutional Review Board (IRB) Application No. Pro2018002356 and performed in line with the IRB recommended guidelines.

REFERENCES

- [1] M. A. Sami, M. Tayyab, P. Parikh, H. Govindaraju, and U. Hassan, "A modular microscopic smartphone attachment for imaging and quantification of multiple fluorescent probes using machine learning," *Analyst*, vol. 146, pp. 2531–2541, 2021, doi: [10.1039/D0AN02451A](https://doi.org/10.1039/D0AN02451A).
- [2] B. V. R. Tata and B. Raj, "Confocal laser scanning microscopy: Applications in material science and technology," *Bull. Mater. Sci.*, vol. 21, no. 4, pp. 263–278, Aug. 1998, doi: [10.1007/BF02744951](https://doi.org/10.1007/BF02744951).
- [3] M. A. Ahamed, G. Kim, Z. Li, and S.-J. Kim, "Pre-programmed microdroplet generator to control wide-ranging chemical concentrations," *Analytica Chimica Acta*, vol. 1236, 2022, Art. no. 340587.
- [4] A. Raj, P. van Den Bogaard, S. A. Rifkin, A. van Oudenaarden, and S. Tyagi, "Imaging individual mRNA molecules using multiple singly labeled probes," *Nature Methods*, vol. 5, no. 10, pp. 877–879, Oct. 2008.
- [5] A. Roda, E. Michelini, M. Zangheri, M. Di Fusco, D. Calabria, and P. Simoni, "Smartphone-based biosensors: A critical review and perspectives," *TrAC Trends Anal. Chem.*, vol. 79, pp. 317–325, 2016.
- [6] Y. Liu, A. M. Rollins, R. M. Levenson, F. Fereidouni, and M. W. Jenkins, "Pocket MUSE: An affordable, versatile and high-performance fluorescence microscope using a smartphone," *Commun. Biol.*, vol. 4, no. 1, Mar. 2021, Art. no. 334.
- [7] A. Bhardwaj, J. Kaur, M. Wuest, and F. Wuest, "In situ click chemistry generation of cyclooxygenase-2 inhibitors," *Nature Commun.*, vol. 8, no. 1, Feb. 2017, Art. no. 1.
- [8] H. C. Koydemir et al., "Rapid imaging, detection and quantification of giardia lamblia cysts using mobile-phone based fluorescent microscopy and machine learning," *Lab Chip*, vol. 15, pp. 1284–1293, 2015, doi: [10.1039/C4LC01358A](https://doi.org/10.1039/C4LC01358A).
- [9] Y. Sung, F. Campa, and W.-C. Shih, "Open-source do-it-yourself multi-color fluorescence smartphone microscopy," *Biomed. Opt. Exp.*, vol. 8, no. 11, pp. 5075–5086, Nov. 2017.
- [10] N. N. Watkins et al., "Microfluidic CD4+ and CD8+T lymphocyte counters for point-of-care HIV diagnostics using whole blood," *Sci. Transl. Med.*, vol. 5, no. 214, 2013, Art. no. 214ra170.
- [11] C. A. Schneider, W. S. Rasband, and K. W. Eliceiri, "NIH image to ImageJ: 25 years of image analysis," *Nature Methods*, vol. 9, no. 7, pp. 671–675, Jul. 2012.
- [12] M. A. Sami, M. N. Tahir, and U. Hassan, "AQAFI: A bioanalytical method for automated KPIs quantification of fluorescent images of human leukocytes and micro-nano particles," *Analyst*, vol. 148, pp. 6036–6049, 2023, doi: [10.1039/D3AN01166F](https://doi.org/10.1039/D3AN01166F).
- [13] N. Otsu, "A threshold selection method from gray-level histograms," *IEEE Trans. Syst. Man. Cybern.*, vol. 9, no. 1, pp. 62–66, Jan. 1979.
- [14] S. Suzuki and K. be, "Topological structural analysis of digitized binary images by border following," *Comput. Vis., Graph., Image Process.*, vol. 30, no. 1, pp. 32–46, 1985.
- [15] H. Govindaraju, M. A. Sami, and U. Hassan, "Machine learning enabled leukocyte quantification using smartphone coupled 3D printed microfluidic biosensor," *IEEE Access*, vol. 10, pp. 85755–85763, 2022.